Human Molecular Genetics, 2016, Vol. 25, No. 6 1152–1164

doi: 10.1093/hmg/ddv638
Advance Access Publication Date: 5 January 2016
Original Article

ORIGINAL ARTICLE

Three-layered proteomic characterization of a novel *ACTN4* mutation unravels its pathogenic potential in FSGS

Malte P. Bartram[1], Sandra Habbig[1,2], Caroline Pahmeyer[1], Martin Höhne[1,7,8], Lutz T. Weber[2], Holger Thiele[4], Janine Altmüller[3,4], Nina Kottoor[5], Andrea Wenzel[3], Marcus Krueger[6,7], Bernhard Schermer[1,7,8], Thomas Benzing[1,7,8], Markus M. Rinschen[1,7,8,†,*] and Bodo B. Beck[3,†,*]

[1]Department II of Internal Medicine and Center for Molecular Medicine Cologne, University of Cologne, Cologne, Germany, [2]Department of Pediatrics, [3]Institute of Human Genetics, [4]Cologne Center for Genomics (CCG), [5]Department of Radiology, [6]Institute for Genetics, [7]Cologne Excellence Cluster on Cellular Stress Responses in Aging-Associated Diseases (CECAD) and [8]Systems Biology of Ageing Cologne, University of Cologne, Cologne, Germany

*To whom correspondence should be addressed at: Department II of Internal Medicine and Center for Molecular Medicine, University of Cologne, Kerpener Str. 62, 50937 Cologne, Germany. Tel: +49 221 478 84443; Email: markus.rinschen@uk-koeln.de (M.M.R.); Institute of Human Genetics, Kerpenerstr. 62, 50937 Cologne, Germany. Tel: +49 221 478 86824; Fax: +49 221 478 86812; Email: bodo.beck@uk-koeln.de (B.B.B.)

Abstract

Genetic diseases constitute the most important cause for end-stage renal disease in children and adolescents. Mutations in the *ACTN4* gene, encoding the actin-binding protein α-actinin-4, are a rare cause of autosomal dominant familial focal segmental glomerulosclerosis (FSGS). Here, we report the identification of a novel, disease-causing *ACTN4* mutation (p.G195D, *de novo*) in a sporadic case of childhood FSGS using next generation sequencing. Proteome analysis by quantitative mass spectrometry (MS) of patient-derived urinary epithelial cells indicated that ACTN4 levels were significantly decreased when compared with healthy controls. By resolving the peptide bearing the mutated residue, we could proof that the mutant protein is less abundant when compared with the wild-type protein. Further analyses revealed that the decreased stability of p.G195D is associated with increased ubiquitylation in the vicinity of the mutation site. We next defined the ACTN4 interactome, which was predominantly composed of cytoskeletal modulators and LIM domain-containing proteins. Interestingly, this entire group of proteins, including several highly specific ACTN4 interactors, was globally decreased in the patient-derived cells. Taken together, these data suggest a mechanistic link between ACTN4 instability and proteome perturbations of the ACTN4 interactome. Our findings advance the understanding of dominant effects exerted by *ACTN4* mutations in FSGS. This study illustrates the potential of genomics and complementary, high-resolution proteomics analyses to study the pathogenicity of rare gene variants.

Introduction

Most children and at least 10% of adults requiring renal replacement therapy and transplantation suffer from inherited, mostly rare kidney disease (RKD) (1). RKD form a highly heterogeneous group with over 200 different monogenic causes. Primary, genetic forms of focal segmental glomerulosclerosis (FSGS) and the

[†]M.M.R. and B.B.B. shared senior and corresponding authorship.

Received: October 18, 2015. **Revised:** December 23, 2015. **Accepted:** December 31, 2015

nephronophthisis complex represent the two most frequent causes of end-stage renal disease (ESRD) up to the age of 25 years (2,3). Especially in ESRD, a correct genetic diagnosis can be challenging given the overlap of clinical, imaging and biopsy findings. Next-generation sequencing (NGS) technologies driven approaches provide the means for establishing a molecular diagnosis for disorders that are too rare to be recognized with certainty or those that are difficult to distinguish from one another (4). Several publications have demonstrated the power of an unbiased, genotype-driven approach to identify the underlying genetic cause even in sporadic cases (5,6). In patients with RKD awaiting kidney transplantation (KTX), genetic screening in order to identify the underlying diagnosis is strongly recommended not only for counseling, but also in order to assess the recurrence risk after transplantation (7).

Primary FSGS is characterized by steroid-resistant proteinuria, hypertension and focal sclerosis of the glomeruli, regularly leading to renal failure and ESRD. *ACTN4* mutations were discovered as the first genetic cause of late onset autosomal dominant familial FSGS where patients typically come to medical attention at early adulthood (8,9). Altogether *ACTN4*-associated FSGS is comparatively rare with only 12 known definite mutations, among them 8 missense variants (HMGD professional database 2015.4).

ACTN4 is a gene product specifically enriched in podocytes, a specialized glomerular cell type maintaining the renal filtration barrier. ACTN4, however, is also abundantly expressed in fibroblasts and epithelial cells (10–13). ACTN4 is an actin-binding and cross-linking protein (14,15). It is essential for a number of important cellular functions, among these are podocyte adhesion (16), fibroblast force generation (12) and signal transduction (17). ACTN4 is also suggested to orchestrate intracellular protein complexes linking the cytoskeleton to the membrane-localized cell–cell contacts (18,19).

Most human ACTN4 mutations localize to the N-terminal actin-binding calponin homology (CH) domain (8,20). Many ACTN4 mutant proteins exhibit an increased affinity to F-actin and form cellular aggregates, which modulate the cytoskeletal function and cellular signalling transduction (21–23).

Here, we report the complementary use of gene panel driven variant identification and unbiased quantitative MS in a case of juvenile non-syndromal ESRD. The aim of this study was to comprehensively characterize the molecular perturbations exerted by the likely pathogenic, but initially unclear *de novo* variant p.G195D *ACTN4*.

Results

Clinical and genetic findings

A 13-year-old girl was hospitalized with symptomatic arterial hypertension, ocular pain and nausea. The patient presented with pleural effusions and moderate ascites in the absence of peripheral oedema. Laboratory investigations revealed ESRD (serum creatinine: 853.6 µmol/l, estimated glomerular filtration rate according to Schwarz: 5.7 ml/1.73 m²/day) and renal anaemia (haemoglobin: 7.5 g/dl). Urine analysis showed a proteinuria of 2.3 g/m²/day with serum albumin in the normal range. Comprehensive serological analysis was unremarkable. Ultrasonography revealed small hyperechoic kidneys with severely reduced corticomedullary differentiation (Fig. 1B). As renal function did not recover, peritoneal dialyses was initiated 48 h after admission and continued for 12 months until the patient received living-donor KTX from her father. The only child of unrelated German parents was the product of natural conception with uneventful normal pregnancy and delivery. She was born small for gestational age with a birthweight of 2.3 kg (at 37 weeks of gestational age). Her further past medical history was unremarkable. Family history was uneventful.

As targeted Sanger sequencing of *NPHS2* and *HNF1B*, two common Mendelian RKD disorders, was negative, we performed gene panel analysis containing 4813 disease-associated genes (Illumina TruSight one, called the 'Mendeliome', mean coverage 101×) in the patient (II-1, Fig. 1C). Next, the data were filtered for potentially deleterious homozygous, compound heterozygous or heterozygous variants in all 4813 genes, including 208 genes associated with RKD (Fig. 1C, Supplementary Material, Tables S1). No truncating mutations were identified. There were only two heterozygous missense variants that were compatible with a non-syndromal RKD phenotype and capable of inducing childhood ESRD: p.G195D in *ACTN4* and p.P1109S in *COL4A3*. A third heterozygous variant was found in *NOTCH2*, a gene associated with Alagille syndrome (24). Segregation analysis by Sanger sequencing of the index patient and both healthy parents for these three variants confirmed *de novo* occurrence of the *ACTN4* mutation (c.1038C>G, p.G195D) in the patient (Fig. 1D). The predicted damaging *ACTN4* variant p.G195D could neither be found in the large public whole exome sequencing (WES) databases nor in our in-house databases (511 exomes and 189 Illumina TruSight one gene panels used to detect pipeline-related artefacts) (see 'Materials and Methods' section, Supplementary Material, Table S1). Both the *COL4A3* variant, found in 0.4% of the population, as well as the *NOTCH2* variant were inherited from the healthy mother, thereby excluding pathogenicity at large.

Functional consequences of ACTN4 G195D mutation

To elucidate the functional consequences of the ACTN4 G195D mutation, we introduced this mutation into ACTN4 expressing plasmids. In stable podocyte cell lines, ACTN4 wild-type (WT) localized to the cell membrane and to membrane ruffles, as described before (13,21,22). In contrast, ACTN4 G195D showed a severely altered localization with multiple, F-actin positive aggregates (Fig. 1E). A similar phenotype was found upon transient transfection in HeLa cells (Supplementary Material, Fig. S1). Further immunofluorescence experiments of the podocyte cell lines using the lysosome marker Lamp1 and the autophagosome marker LC3 showed no significant overlap with the ACTN4 G195D aggregates (Supplementary Material, Fig. S2). Analysis of the migrational behaviour, a known readout of cytoskeletal actin dynamics, revealed a slight slow-down of migration in the ACTN4 G195D cell line versus ACTN4 WT cell line (Supplementary Material, Fig. S3A and C). We performed phalloidin staining of these migrated cells and could verify the mutant-induced actin aggregation (Supplementary Material, Fig. S3B). We also applied a biochemical fractionation assay using differential centrifugation (21) to human epithelial kidney (HEK293T) cells expressing F.ACTN4 WT or G195D (Supplementary Material, Fig. S4A and B). Immunoblot analysis revealed that the G195D protein is triton insoluble, indicating a strong association with large actin bundles.

Analysis of primary renal epithelial cells derived from the patient

To further analyse the mutation, we obtained renal epithelial cells from patient urine following a recently published protocol (25). Three different clones of primary kidney epithelial cells were generated from the patient, and compared with three independent clones obtained from three healthy controls. All experiments were performed with passage 2 or 3 of the cells

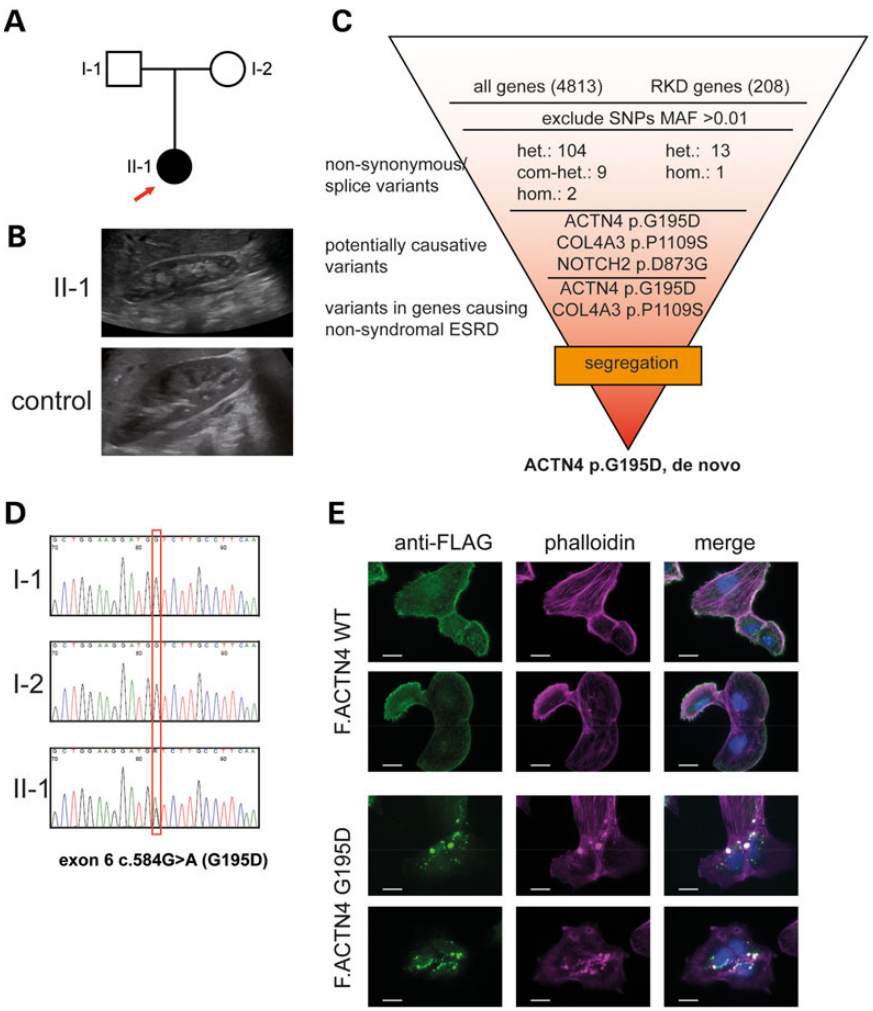

Figure 1. (**A**). Pedigree of the index patient. (**B**). Ultrasound examination shows small and hyperechoic kidneys (length: 6.43 cm) in comparison to a healthy weight- and sex-matched control kidney ultrasound. (**C**). Analysis workflow of the gene panel that lead to the identification of the causative mutation in the index patient. Of note, no truncating mutations were identified (**D**). Targeted Sanger sequencing of *ACTN4* exon 6. Electropherograms depict the relevant sequence section around c.584G>A (p.G195D) in the index patient (II-1) and her parents. (**E**). Immunofluorescence analysis of podocyte cell lines stably expressing FLAG-tagged ACTN WT or G195D. The mutant protein shows severe mislocalization and marked alterations of the actin cytoskeleton (bar = 20 µm).

without any immortalization procedures or transduction of genetic information to the primary cells.

We subjected these samples to proteomic analysis. Hierarchical clustering revealed a clear separation of the three primary patient cell clones from the three control cell clones (Fig. 2A). We identified 3952 proteins with high confidence, including several epithelial markers (Supplementary Material, Fig. S5A). We found that the sequence coverage of ACTN4 within this data set was 75.4% (Supplementary Material, Fig. S5B). It is pertinent that resolving and quantifying the mutated and WT peptide would allow investigating the differential expression of both ACTN4 forms in the patient cells. In fact, we confidently sequenced the 'WT peptide', as well as the 'mutated peptide' (Fig. 2B). As shown in the violin plot of logarithmic MS1 peptide intensities, the overall intensity of all ACTN4 peptides was lower in the patient cells (Fig. 2C). The protein fragment encoded by the WT allele had much higher intensity as the protein fragment bearing the G195D mutation. The 'G195D peptide' was detected at very low intensities—close to the detection limit—in the patient samples, but not in the control samples (Fig. 2C). Thus, the mutation does not only alter the localization of the protein, but also leads to a reduced expression of ACTN4.

In silico and *in vitro* characterization of ACTN4 G195D stability

The G195D mutation is localized in one of the CH domains of ACTN4, together with several previously described mutations [e.g. K255E (8,26)]. G195 is not solvent-accessible. To assess the biophysical impact of a G>D exchange within the molecule, we used molecular dynamics analyses based on the solved crystal structure of the CH domain (Fig. 3A). All algorithms and platforms predicted a strong biophysical decrease of stability caused by introduction of the amino acid exchange G195D (Table 1) (61–66). Similar results were obtained for the solved, highly conserved structures of ACTN1 and 3 (27–29). Consistently, expression of ACTN4 G195D in HEK293T cells was reduced (Fig. 3B). Since this experiment was performed in a heterologous overexpression system, stability assays in the stable podocyte cell lines were performed in addition. Incubation with cycloheximide

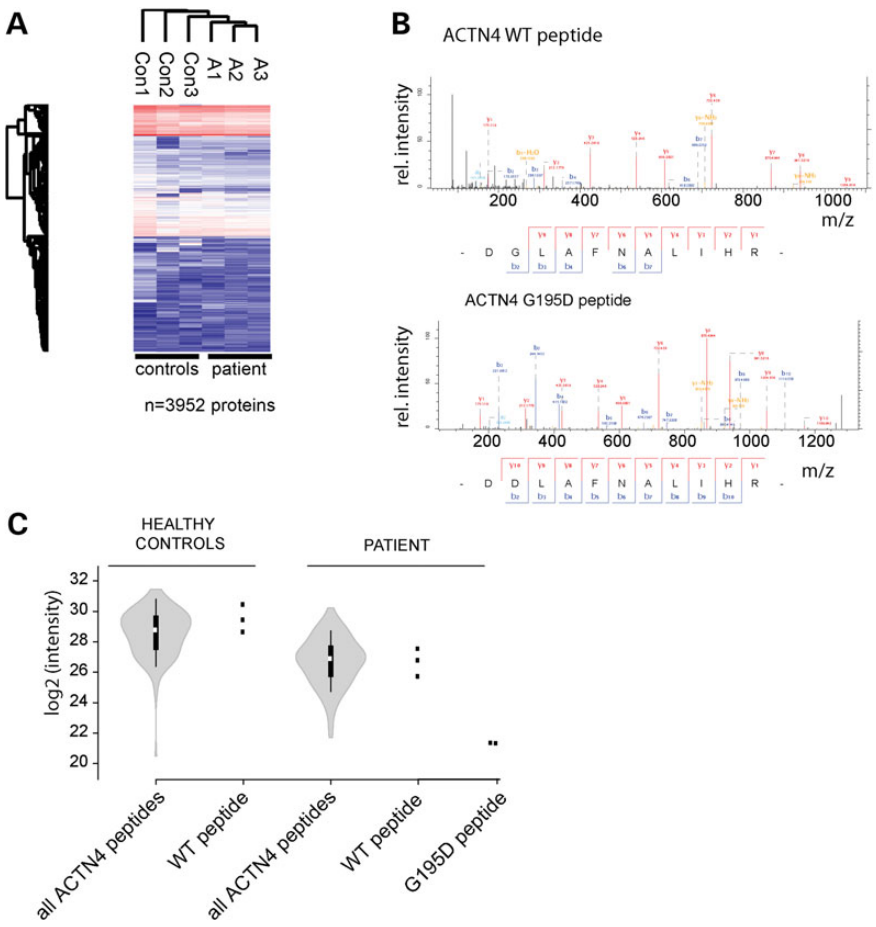

Figure 2. Characterization of primary epithelial cells derived from the patient's urine reveals that ACTN4 G195D is less abundant than the WT protein. (**A**). Overview and hierarchical clustering of approximately 4000 proteins within patient and control samples. (**B**). MS2 spectra ('sequences') of a peptide showing the WT version of the protein as well as the 'diseased' (G substituted to D) version of the protein. Only the WT but not the G195D version of the protein was discovered in all patient material (both patient and control). (**C**). MS1 intensities of peptides derived from ACTN4 as a violin plot. White circles show the medians; box limits indicate the 25th and 75th percentiles as determined by the R software; whiskers extend 1.5 times the interquartile range from the 25th and 75th percentiles; polygons represent density estimates of data and extend to extreme values. The replicates of the discovery of the 'WT' peptide as well as the 'disease' peptide were plotted. The 'disease' peptide has by far lower intensities when compared with all other ACTN4 peptides (who are shared between mutant and WT protein).

(CHX), an inhibitor of translation, resulted in a stronger decay of ACTN4 G195D protein expression when compared with ACTN4 WT protein (Fig. 3C).

Proteomic analysis of ACTN4 ubiquitylation

Decreased stability of a dysfunctional protein can be mediated by increased ubiquitylation. Ubiquitin remnants are indicative of protein ubiquitylation and can be localized and quantified using proteomics (30). In this analysis, the G195D mutant (expressed in HEK293T cells) showed a large increase in ubiquitylation at several lysines. Interestingly, the adjacent lysine residues (K214 and K217) show the largest increase (Fig. 4A). In addition, one ubiquitylation site resided just two amino acids N-terminal from G195D (K193, Fig. 4B). We also performed the corresponding experiment in cell culture followed by western blot analysis and could demonstrate an increase in ubiquitylation of ACTN4 G195D when compared with WT (Fig. 4C).

Patient cell proteome and ACTN4 interactome

We then performed a global scale proteomic analysis of the patient cells. In total 2637 proteins were quantified. Consistent with the previously shown results on the peptide level (Fig. 2) ACTN4 was the most significantly decreased protein within the patient cells (Fig. 5A). In total 116 proteins were significantly changed (Supplementary Material, Table S2). A gene ontology (GO) term enrichment analysis of the changed proteins (when compared with the unchanged proteins) is depicted in Supplementary Material, Figure S6A and B.

There was a uniform, global decrease of proteins containing a LIM domain in patient cells (Fig. 5B). The decreased LIM-domain proteins included ZNF185, PDLIM4, LMO7, LIMA1 and CRSP. Other LIM-domain proteins (including PDLIM1, 2 and 7) were decreased as well, but at lower ratios.

We hypothesized that the dissection of the ACTN4 interactome will illuminate a mechanistic link between the ACTN4 mutation and the coregulated proteins. We used podocytes with stable expression of ACTN4 WT and G195D and performed analyses of the interactomes when compared with a GFP expressing control cell line (Fig. 5C). The analysis revealed that ACTN4 was the most enriched and most significant protein among more than 2000 quantified proteins. Interestingly, coenriched interactors included several proteins whose expression was decreased in the primary patient cells. This included the PDLIM proteins PDLIM1, 2, 4 and 7 as well as the LIM-domain protein ZNF185 (Fig. 5A and C). All interactors are depicted in Table 2. On a

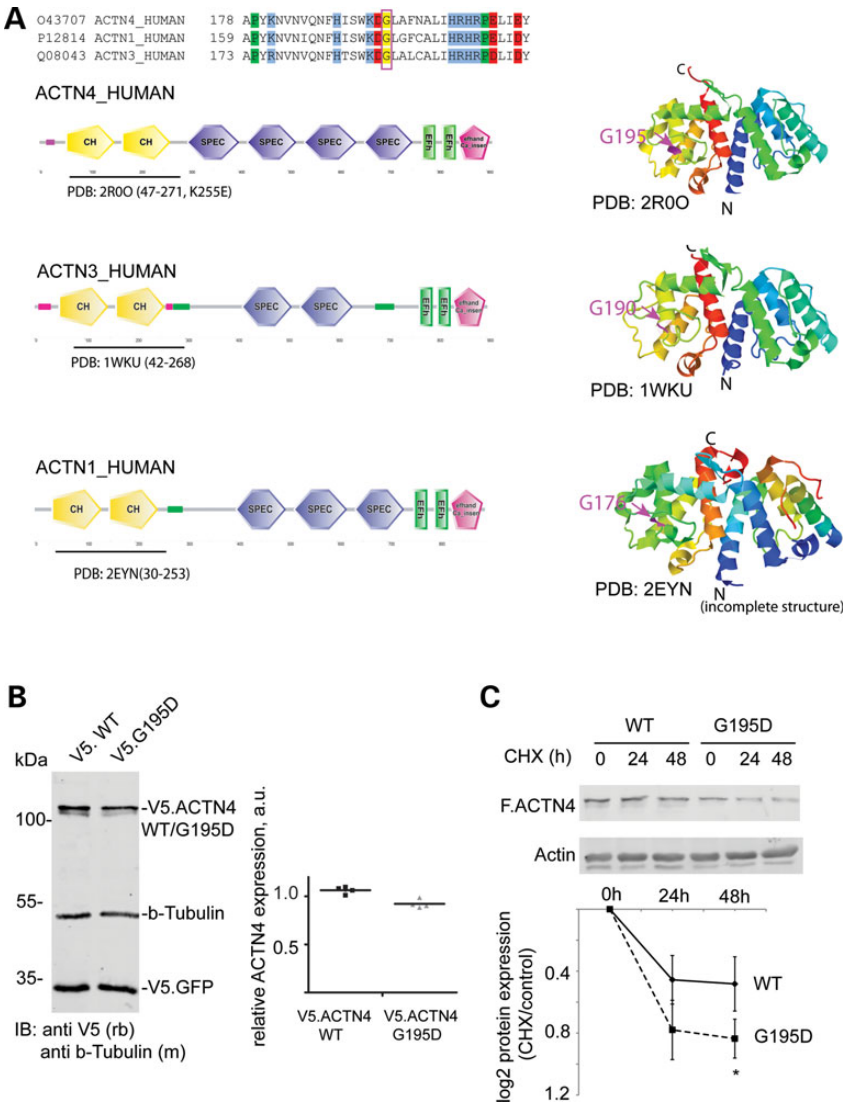

Figure 3. *In silico* and *in vitro* characterization of the G195D ACTN4 mutation. (**A**). Alignment of ACTN4 with the highly similar proteins ACTN1 and ACTN3. The amino acid G195 (yellow mark and magenta box) resides in the first CH domain of ACTN4, which is highly conserved among ACTN1, 3 and 4 (left side). The solved crystal structures for ACTN1, 3 and 4 are shown on the right side. The residue aligning with G195 is highlighted in magenta. It is not solvent accessible. (**B**). V5.ACTN4 WT or G195D and V5.GFP were cotransfected into HEK293T cells. WCLs were subjected to SDS–PAGE, and membranes were stained for beta Tubulin (loading control) and V5. Densitometry reveals that G195D is less expressed than ACTN4 WT ($n = 4$, $^*P < 0.05$, two-tailed *t*-test) (**C**). Pulse chase assays of F.ACTN4 WT and G195D stably expressed in human podocytes. Cells were treated with CHX ($c = 50$ µg/ml) for the indicated time points. Western blot analysis followed by densitometry revealed a stronger decay of G195D expression when compared with WT protein ($n = 5$, error bars indicate SEM, $^*P < 0.05$, two-tailed *t*-test).

Table 1. The effect of G to D mutation on α-actinin protein stability (ΔΔG) using 5 different software prediction methods

Platform	PDB: 1WKU (ACTN3) ΔΔG (kcal/mol)	Effect	PDB: 2R0O (ACTN4) ΔΔG (kcal/mol)	Effect	PDB: 2EYN (ACTN1) ΔΔG (kcal/mol)	Effect
Cupsat (61)	−7.13	Destabilizing	−6.63	Destabilizing	−5.39	Destabilizing
Eris (62)	>10	Destabilizing	>10	Destabilizing	>10	Destabilizing
IMutant 2.0 (63)	−2.55	Destabilizing	−2.38	Destabilizing	−2.64	Destabilizing
POPMUSIC (64,65)	3.44	Destabilizing	3.26	Destabilizing	3.39	Destabilizing
DUET (66)	−2.807	Destabilizing	−2.486	Destabilizing	−2.362	Destabilizing

Solvent accessibility of G195 residue (all models): 0 (buried residue).

bioinformatics level, the interacting proteins were statistically enriched for ion and GTP-binding proteins, for focal adhesion proteins, as well as proteins carrying PDZ and LIM domains (Supplementary Material, Fig. S7). We performed a corresponding analysis for the interactome of G195D. Consistent with the ACTN4 expression data in podocytes (Fig. 3C), overall signals of immunoprecipitated ACTN4 G195D were reduced compared with WT (Fig. 5D). Only ACTN4 and the four-and-a-half LIM

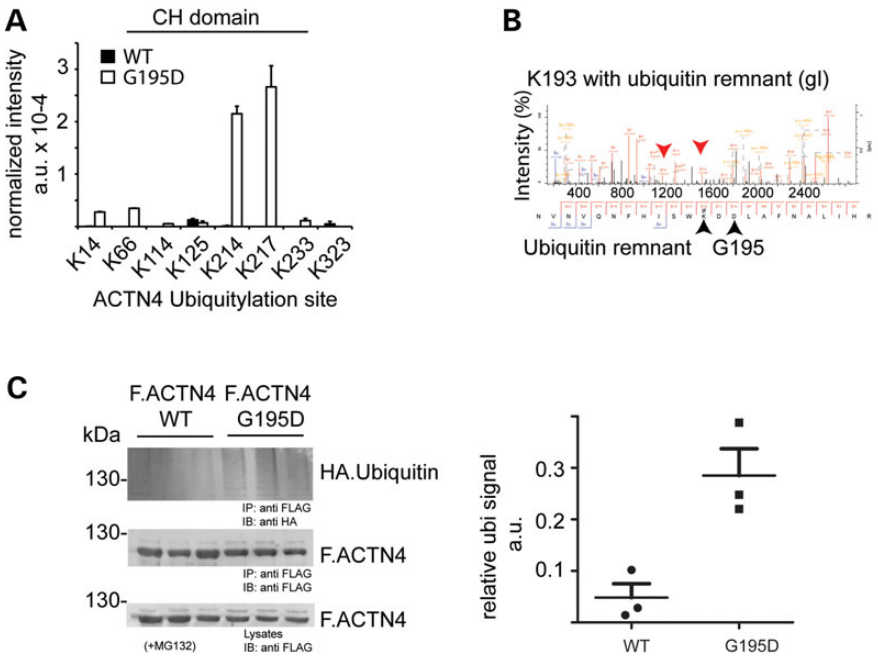

Figure 4. Analysis of ubiquitylation of ACTN4 G195D when compared with WT in cell culture in the presence of a proteasome inhibitor (MG132, 10 µg/ml). (**A**). MS analysis of ubiquitin remnants on ACTN4 WT and G195D. Ubiquitylation sites of ACTN4 were identified as K-ε-Gly-Gly ubiquitin remnant peptides. MS1 intensities of site containing ubiquitylation sites were normalized against total protein intensity. Error bars indicate SEM, $n = 3$. The majority of all ubiquitylation sites reside within the CH domain. (**B**). MS2 spectrum of an identification of a K-ε-Gly-Gly ubiquitin remnant peptide at K193, two positions N-terminal of the introduced mutation. (**C**). Analysis of ubiquitylation via western blot. Ubiquitin is visible as HA-positive smear with higher molecular weight than the ACTN4 band. Monoubiquitylated ACTN4 is distinguishable. Densitometry of the experiment shows a strong increase in ubiquitylation. Densitometric signal of ubiquitin was normalized against F.ACTN4 signal ($n = 3$, error bars indicate SEM, $^*P < 0.05$, two-tailed *t*-test).

domains protein (FHL2) were significantly enriched in the 'disease protein interactome', using the same statistical parameters as for the WT interactome. A correlation plot of fold changes in protein intensities in the immunoprecipitation samples is depicted in Figure 5E.

Next, analysis of absolute abundances of proteins in the pulldowns was performed (31–33). In both cases, ACTN4 was the major enriched protein within the complex (Fig. 5F). The LIM-domain proteins PDLIM1, 2, 4 and 7 and ZNF185 were identified as the major interactors within the protein complex. Proteins without LIM domains such as RHOC and synaptopodin were represented only in a substoichiometric abundance. ZNF185 and FHL2 copy numbers were significantly increased within the G195D immunoprecipitated complex.

Discussion

Most rare disorders are caused by mutations in genes, which encode known proteins and many genes have already been associated with Mendelian disease. Therefore, massive parallel sequencing approaches provide the means for establishing a genetic diagnosis in a cost-effective and timely manner, but the identification of the underlying genetic cause in sporadic cases from non-consanguineous families remains challenging (34,35). Another problem is the substantial rate of false-positive mutations, that are polymorphisms or rare benign variants, and also false-negative variants reported in the literature and recorded in mutational databases (36,37). If diagnostic decision-making is based on incorrect assumptions, it can lead to severe clinical consequences. This challenge, already noted in the pre-NGS era, is likely to increase with multiple testing performed in whole exome/genome sequencing or use of gene panels. Large databases like the Exome Aggregation Consortium (ExAC) browser can partially solve this problem by assessing the frequency of allegedly pathogenic variants in the general population.

Thus, novel, putatively causative variants often lack the strength to prove positive alone in the absence of further genetic and functional evidence. Of note, even rare homozygous variants resulting in protein truncation may have no clinical sequela, so potentially causative variants for rare disorders must be interpreted with great caution (38).

In our patient with a phenotype of juvenile onset proteinuria and ESRD a genetic cause was most likely. NGS sequencing of 4813 genes identified with p.G195D *ACTN4*, a novel potential mutation. Further genetic analyses revealed *de novo* occurrence of p.G195D in the index case, whereas the other two candidate variants in *COL4A3* and *NOTCH2* were inherited from the healthy mother.

In summary, there was sufficient evidence for G195D *ACTN4* being the underlying mutation in our patient: (i) the variant was rare and could not be found in any database; (ii) it affected a highly conserved residue and the mutation was predicted to be pathogenic by several bioinformatic algorithms; (iii) it occurred *de novo* (39). Given the low stochastic frequency of true *de novo* single-nucleotide variants (SNVs) of ca. 1.12 per whole exome (5), it is highly unlikely that another mutation was associated with this non-syndromal RKD phenotype. Finally, the phenotype of childhood onset *ACTN4*-associated FSGS has been reported previously, although most patients affected by *ACTN4* mutations show a milder clinical course (20). It is pertinent to note that the mutation may also affect renal development, which may ultimately contribute to ESRD.

To further elucidate the molecular pathogenicity of p.G195D *ACTN4* we used three unbiased, complementary proteomic strategies. This involved (i) analysis of the proteome in native,

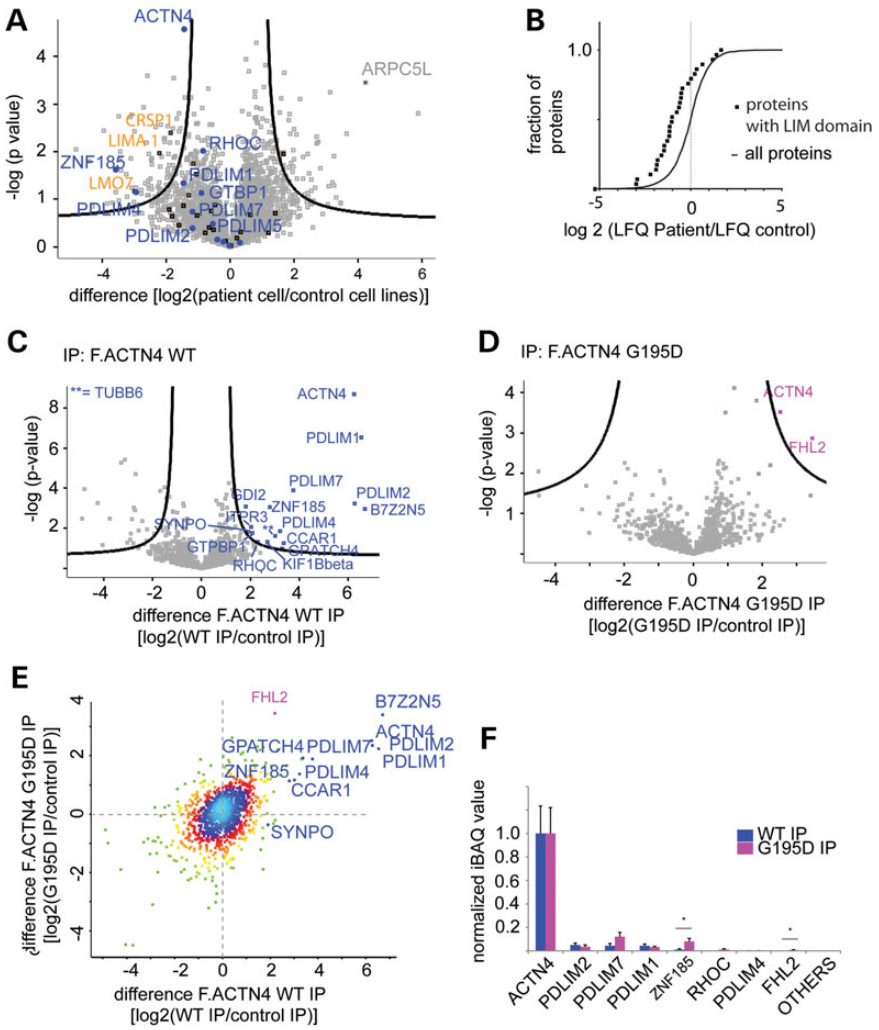

Figure 5. Analysis of the primary patient cells and the ACTN4 interactome suggests an impact of ACTN4 G195D onto the ACTN WT interactome. (**A**). Volcano plot demonstrating differences between patient cells and control cells. Each dot represents a protein. The *P*-value of a two-sided *t*-test is plotted against the logarithmic fold change between the two groups. ACTN4 was decreased in patient cells with high significance. Interactors of ACTN4 (determined by Fig. 5C) are labelled as blue. Proteins containing LIM domains are labelled as orange with black borders. (**B**). Cumulative histogram demonstrating global down-regulation of LIM-domain proteins within the patient cells as compared to the control cells. The distribution difference was significantly different ($P = 1.95 \times e^{-10}$) in a two-sided Kolmogorov–Smirnov test. (**C**). Volcano Plot of a MS/MS analysis of immunoprecipitated F.ACTN4 WT when compared with control. FLAG-pulldowns from F.ACTN4 WT as well as GFP (control) expressing podocytes were subjected to MS/MS analysis. Each dot represents a protein. The significance of differential abundance in a two-tailed *t*-test was plotted against the logarithmic expression values depicted as ratio (F.ACTN4 pulldown/control pulldown). ACTN4 was among the strongest and the most significantly enriched protein within the pulldown. All proteins passing the statistical criterion for significance are labelled with their gene symbol (in blue). (**D**). Volcano plot of an immunoprecipitated ACTN4 G195D when compared with control. The data presentation is analogue to Figure 5A. Since overall expression of the protein is lower, significances as well as fold-enrichment are lower for the ACTN4 protein. FHL2 is the only interactor passing the statistical criterion (in magenta). (**E**). Comparison of relative enrichment of ACTN4 immunoprecipitation in WT and G195D conditions. The analysis reveals similar enrichment of interactors. FHL2, however, appears to have relatively stronger enrichment in the pulldown of G195D. (**F**). Analysis of complex stoichiometry. iBAQ, a parameter correlating to absolute protein abundance within a sample, was used to normalize ACTN4 copy numbers to 1. ACTN4 is the most abundant protein within the sample. PDLIM1, 2 and 7 are stronger interactors, the rest of proteins is found in a substoichiometric part in the complex. ZNF185 had higher iBAQ values in F.ACTN4 G195D pulldown when compared with F.ACTN4 WT pulldown ($n = 6$, error bars indicate SEM, $^*P < 0.05$, two-tailed *t*-test).

patient-derived cells, (ii) analysis of the ACTN4 ubiquitylation and (iii) analysis of the ACTN4 interactome.

Primary patient material of the affected organ or tissue is often not available. Recent studies opened a novel promising, non-invasive method to obtain primary renal epithelial cells by collecting urine and to selectively grow renal epithelial cells (25,40). We compared patient-derived cells harboring the p.G195D-mutation to three independent healthy controls. The cells—selected by specific, nutrient rich medium according to a previously established protocol (25)—expressed several markers for epithelia, without expressing any of the high-abundant podocyte markers (Nephrin, Podocin and WT1). The expression of epithelia markers (Supplementary Material, Fig. S5A) was not different between patient and control cell lines.

Using these cell lines it was possible to resolve the peptide carrying the mutation, with the G195D-containing peptide only being identified within the patient sample (Fig. 2B and C). We found that the G195D allele was significantly less expressed not only compared with the control cells, but also compared with its own, intrinsic control—the WT allele of the patient-derived cells. This allele-specific resolution on the proteome level allows a direct comparison of the functional consequences of a mutation.

Table 2. Outline of the ACTN4 interactome in podocytes

Uniprot	Gene names	Protein names	log2 (fold change) WT IP	−log (P-value) WT IP	log2 (fold change) G195D IP	−log (P-value) G195D IP	LIM domains	Amino acids
O43707	ACTN4[a]	α-actinin-4[a]	6.25	8.68	2.52	3.52	N/A	912
V9HW92	PDLIM1	PDZ- and LIM-domain protein 1	6.53	6.55	2.24	2.19	1	329
Q96JY6	PDLIM2	PDZ- and LIM domain protein 2	6.27	3.23	2.36	0.79	1	352
Q9NR12	PDLIM7	PDZ- and LIM domain protein 7	3.77	3.90	1.89	1.98	3	458
Q5T3I0	GPATCH4	G patch domain-containing protein 4	3.37	1.26	1.93	0.41	N/A	446
Q4R9M7	KIF1B	Kinesin-like protein KIF1B	3.32	0.97	1.89	0.34	N/A	1783
P50479	PDLIM4	PDZ- and LIM domain protein 4	3.22	1.85	1.37	0.88	1	330
Q8IX12	CCAR1	Cell division cycle and apoptosis regulator protein 1	3.01	1.62	1.18	0.50	N/A	1150
O15231	ZNF185	Zinc finger protein 185	2.79	3.05	1.14	1.14	1	690
Q9BUF5	TUBB6	Tubulin beta-6 chain	2.69	1.31	1.66	0.59	N/A	446
P08134; P61586	RHOC/ RHOA	Rho-related GTP-binding protein RhoC/RhoA	2.31	1.30	2.21	1.05	N/A	193
B0QY59	GTPBP1	GTP-binding protein 1	2.10	1.77	1.28	0.68	N/A	669
Q59ES2	ITPR3	Inositol 1,4,5-trisphosphate receptor type 3	2.05	2.07	1.65	0.84	N/A	2262
A7MD96	SYNPO	Synaptopodin	1.91	1.83	−0.36	0.15	N/A	904
Q6IAT1	GDI2	Rab GDP dissociation inhibitor beta	1.82	3.07	0.48	0.45	N/A	445
Q53T40	FHL2[b]	Four and a half LIM domains protein 2[b]	2.20	1.24	3.46	2.87	4.5	279

[a]Significant in both WT and G195D IP.
[b]Significant only in G195D IP.

Computational biophysical analyses, pulse-chase assays and ubiquitylomic analysis revealed a destabilizing effect of G195D, a finding consistent with reduced expression of this allele in the patient cells. The majority of ubiquitylation sites discovered in the entire protein are in the N-terminal CH domain as is the mutation (Fig. 4A). Interestingly, the sites adjacent to the mutation sites showed a particularly high increase of ubiquitylation. We suggest that the mutation of G195, a buried residue, to a negatively charged aspartate (D), could cause a local unfolding of the protein. This could expose adjacent lysines to ubiquitin ligases.

On a global level, proteomic analysis of the patient cells revealed pathways potentially perturbed by the G195D allele. The key regulated proteins involved not only well-established regulators of the actin cytoskeleton [such as RhoA, Cdc42, EPLIN (also known as LIMA)] (41,42), but also the significant depletion of LIM domain-containing proteins (Fig. 5A and B). Of note, these proteins are also key constitutive elements of the ACTN4 interactome. This implies that the G195D mutation perturbs the remaining ACTN4 WT allele by dysregulating the key interaction partners. Previous data suggest that ACTN4 interacts with LIM-domain proteins via its C-terminus (43). To this end, we did not expect a strong effect of mutations of the N-terminal CH domain on the interactome. This finding is supported by the similar stoichiometry of the ACTN4 WT and G195D interactome (Fig. 5C–E).

An interesting finding was that the protein FHL2 even increased its affinity upon mutation. FHL2 is the smallest protein of all interactors (279 AA) with the most LIM domains (4.5) (Table 2). The LIM domain is a modular interaction domain, and usually one LIM domain is sufficient for the binding of the interaction partner (44). Thus, FHL2 may compete better in the complex when compared with the other interactors. Taken together, the interactome data are consistent with increased degradation, but not mutation-dependent interaction as a crucial mechanism in the pathogenicity of the G195D allele.

Up to date, several hypotheses exist how mutations in *ACTN4* cause FSGS on a molecular level. It has been suggested that mutated ACTN4 is more instable (13), leads to changes in cell adhesion and stiffness of the cytoskeleton (12,21), or causes aggregates that are toxic by themselves (13,21,45). This study is consistent with these hypotheses: the p.G195D mutation causes intracellular aggregates that lead to disturbance of the cytoskeleton (Fig. 1E). Subsequently, the ACTN4 mutation leads to instability via increase in ubiquitylation (Fig. 4). In addition, we add the attractive hypothesis that mutated ACTN4 leads to profound changes in LIM-domain proteins, important modular regulators of cell adhesion (44,46) (Fig. 5). These dysregulated proteins are key components of the ACTN4 interactome thereby explaining the dominant nature of the mutant ACTN4: the WT allele is still abundantly expressed in the cell, but cannot maintain cell homeostasis. We suggest that the observed pathological changes in the patient are not only a direct consequence of the degraded mutant ACTN4 protein, but also of the depletion of its LIM domain interaction partners. These perturbations may be part of a complex response to the mutant protein, and may ultimately contribute to ESRD and possibly defects in renal development.

In conclusion, we combined a NGS-gene-panel ('Mendeliome') based data set with three-layered proteomics. We suggest that the integration of these data reflects the pathogenicity of the mutation. Proteogenomics, the unbiased analysis of the proteome based on NGS data, has already been developed and applied successfully to cancer, a disease with very frequent and disruptive somatic mutations (47). The success of proteogenomics is demonstrated by the clear improvement of cancer classification (48). In the next decade with ever-improving proteomic technologies, time will tell whether such combined 'proteomendeliomic' approaches as described here will be feasible for shaping understanding and classifications in sporadic and inherited Mendelian diseases.

Materials and Methods

Probands

All investigations were conducted in accordance with the principles of the Declaration of Helsinki and after obtaining written

informed consent from the patient and her parents. Clinical and biochemical data were collected from medical charts. Standard methods were used to analyse electrolytes, creatinine and other laboratory parameters. This study was carried out with approval of the ethic committee of the University Hospital Cologne (number 12-204).

Genetic analysis

Genomic DNA was extracted from isolated peripheral blood lymphocytes by standard procedures. We performed gene panel (Illumina trusight one, 4813 genes, called the Mendeliome) analysis in the index patient II-1 followed by NGS on a Illumina MiSeq™ sequencing platform. Filtering and variant calling was performed with the Cologne Center for Genomics (cCG)' VARBANK database and analysis tool (unpublished data, https://varbank.ccg.uni-koeln.de) as described previously (49). In particular, we filtered for high-quality (coverage >15×; phred-scaled quality >25), rare (minor allele frequency ≤0.01) variants based on dbSNP 134, the 1000 Genomes database build 20110521, the public Exome Variant Server, US National Heart, Lung and Blood Institute, build ESP5400 and an in-house database of 511 epilepsy patients.

Mutational analysis of the identified variants in the *ACTN4*, *COL4A3* and *NOTCH2* genes was performed by exon polymerase chain reaction (PCR). Purified PCR products were sequenced by BigDye terminator ready reaction kit v.1.1 (Life Technologies), using a 3500 Genetic Analyzer (Applied Biosystems). Resulting sequences were evaluated with the Sequence Pilot™ software (JSI Medical Systems GmbH, Germany).

Genetic information was obtained from the following sources: National Center for Biotechnology Information (NCBI; http://ncbi.nlm.nih.gov/), UCSC Genome Bioinformatics (http://genome.ucsc.edu/) (50,51), 1000 Genomes Browser (http://1000genomes.org/) (39), Exome Variant Server (http://evs.gs.washington.edu/EVS) accessed in August 2015, ExAC browser [ExAC, Cambridge, MA, USA (URL: http://exac.broadinstitute.org)] accessed in August 2015 and cCG, in-house WES data set (http://varbank.ccg.uni-koeln.de).

Missense variants were subjected to *in silico* analysis using the following tools: MutationTaster (http://www.mutationtaster.org/) (52) and PolyPhen-2 (polymorphism phenotyping v2, http://genetics.bwh.harvard.edu/pph2/). Potential variants affecting splice sites were predicted with the following tools (MaxEntScan, HSF, MutationTaster, SIFT, PolyPhen-2) (53) via Alamut Visual (Alamut Visual version 2.6; Interactive Biosoftware, Rouen, France), all accessed in August 2015.

Cell culture and plasmids

HEK293T and Hela cells were maintained in Dulbecco's modified Eagle's medium (DMEM) supplemented with 10% fetal bovine serum (FBS). Transient transfection of HEK293T cells was carried out using the calcium-phosphate method. The human podocyte cell line was maintained in RPMI medium supplemented with 10% FBS and 1 × insulin-transferrin supplement (54). Human Actinin4 was subcloned from a human fetal brain cDNA library using standard PCR and cloning techniques into a modified pcDNA6 vector (Invitrogen) containing an N-terminal V5 tag. The patient mutation G195D was generated using Quikchange mutagenesis according to standard protocols. All plasmids were verified by sequencing. To generate podocyte cell lines stably expressing ACTN4 WT or G195D we subcloned N-terminal FLAG-tagged ACTN4 WT and G195D into a modified pENT1A vector (Invitrogen) and recombined into pLenti6.3 Dest vectors using the Gateway technology (Invitrogen). After lentivirus production in HEK293T cells the human podocyte cell line was transduced for 24 h. 48 h later blasticidin (10 µg/ml) was added for 7 consecutive days to select the transduced cells. For CHX pulse assays cells were treated with CHX 50 µg/ml in the cell culture medium for indicated period of time. Afterwards, whole cell protein lysates were generated and subjected to immunoblot analysis.

Isolation of primary renal epithelial cells from urine

The generation of the primary renal cells was done as described previously (25). This study was carried out with approval of the ethic committee of the University Hospital Cologne. Written informed consent was obtained from all participating children and their parents. After centrifugation of 100–500 ml of fresh urine (400*g*, 10 min at room temperature) the resulting cell pellet was washed (10 ml PBS + 100 U/ml penicillin, 100 µg/ml streptomycin + 500 ng/ml amphotericinB) and centrifuged again (200*g*, 10 min at room temperature). Afterwards the cell pellet was resuspended in the primary cell medium [DMEM high glucose/HamF12 1:1 mix supplemented with 10% FBS, 100 U/ml penicillin, 100 µg/ml streptomycin, 500 ng/ml amphotericinB and REGM SingleQuotKit supplements (CC-4127, Lonza)] distributed onto a 12-well that was coated before with 0.1% gelatin (wt/vol). One millilitre of the primary cell medium was added per well. Every 24 h 1 ml of the medium was exchanged the following 4 days. Afterwards the medium was changed to the proliferation medium (1:1 mix of RE/MC medium (RE medium (CC-3190 + Supplements; Lonza), MC medium [DMEM high glucose + 10% FBS + 100 U/ml penicillin + 100 µg/ml streptomycin + 1% GlutaMAX + 1% NEAA (Gibco 11140-035) + 5 ng/ml bFGF (Peprotech, cat. no. 100-18B), 5 ng/ml PDGF-AB (Peprotech, cat. no. 100-00AB) + 5 ng/ml EGF (Peprotech, cat. no. AF-100-15)]. All experiments were carried out with non-immortalized cells of passage 2 or 3.

Immunofluorescence

Hela cells that were transfected with the indicated plasmids using Genejuice (Novagen) or the podocyte cell lines were splitted onto coverslips. Twenty-four hours later the cells were washed with PBS and fixed using 4% PFA for 10 min at room temperature. Afterwards the samples were blocked using 5% normal donkey serum in PBS containing 0.1% Triton X-100. After sequential incubation with the primary (anti-V5, Serotec MCA1360 1:1000; anti-FLAG, Sigma F3165 1:2000; anti-LC3, Cell Signaling 2775 1:100; anti-Lamp1, Cell Signaling 9091 1:100) and secondary antibodies (rabbit Cy3, mouse DyLight-488 or mouse DyLight-549, Jackson ImmunoResearch 1:500) and phalloidin (Invitrogen 1:250), the coverslips were mounted using ProlongGold + DAPI (Invitrogen). The cells were analysed using an Axiovert 200 microscope (objective: C-Apochromat 63×/1.22 W) equipped with an Axiocam MRm and the Apotome system (Carl Zeiss MicroImaging, Jena, Germany) using Axiovision 4.8 for acquisition and subsequent image processing (Carl Zeiss MicroImaging).

Actin fractionation assay

To analyse the subcellular distribution of ACTN4 and its association with structures of the actin cytoskeleton differential centrifugation was used as described before (21,55). V5 tagged ACTN4 WT or G195D plasmids were transfected into HEK293T cells using the calcium phosphate method. The following day, cells were harvested in ice-cold PBS and lysed with lysis buffer containing 1% Triton X-100 [1% Triton X-100, 20 mM Tris–HCl, pH

7.5, 50 mM NaCl, 50 mM NaF, 15 mM $Na_4P_2O_7$, 2 mM Na_3VO_4 and PIM complete (protease inhibitor mix; Roche)]. Afterwards the input [whole cell lysate (WCL)] fraction was taken. After low-speed centrifugation at 14.000 × *g* for 15 min the Triton-X insoluble (TI) fraction containing large cytoskeletal structures like actin bundles remains in the pellet. The supernatant containing the Triton-X soluble (TS) fraction was further processed with centrifugation at 100.000 × *g* for 30 min to separate the F-actin (pellet, P) and soluble G-actin (supernatant, S) fractions. The fractions were subjected to western blot analyses with the indicated antibodies. Densitometry was performed using ImageJ. Depicted are the densitometric fractions in comparison with the total signal. The experiment was repeated three times, analysis was performed using a paired Students *t*-test.

Migration assay

The podocyte cell lines transduced with FLAG-tagged ACTN4 WT or G195D were seeded at equal numbers onto 35 mm µ-dishes with culture insert (Ibidi). The cells were allowed to attach for at least 48 h. Afterwards the experiment was started by removing the culture insert. Pictures were taken in the incubator using a JuLi live cell imager (Digital Bio) at 33 or 37°C, respectively. For the 37°C condition the cells were differentiated for at least 7 days a 37°C before the experiment was started. The area covered after 8 h of migration was manually outlined and measured using ImageJ. Quantification is depicted in the graph in Supplementary Material, Figure S3C as percent of the total migration area covered by the respective cell line. The experiment was repeated four times at both temperatures, analysis was performed using a paired Students *t*-test.

Analysis of thermodynamic stability (delta-delta-G) *in silico*

The respective PDB files were obtained from the Pubmed structure. Since there is no crystal structure for WT ACTN4 available, we used the structure of ACTN4 K255E, which shows no significant structural change in comparison with the WT protein (27). The files were uploaded to the respective webservers and calculation of free energy [delta-delta-G (ΔΔG)] was performed using the default settings. The effect of an amino acid substitution (G to D, for respective residues see Fig. 3A) was calculated.

Sodium dodecyl sulphate–polyacrylamide gel electrophoresis and immunoblotting

Equal amounts of protein were separated by sodium dodecyl sulphate–polyacrylamide gel electrophoresis (SDS–PAGE) and blotted onto a polyvinylidene difluoride-low-fluorescence membrane. After blocking with 1 × Rothiblock (Roth), membranes were incubated with primary antibody in PBST (PBS with 0.1% Tween; rabbit anti-FLAG Sigma F7425 1:1000, mouse anti-FLAG Sigma F3165 1:10000, rabbit anti-V5 Millipore AB3792 1:2000, mouse anti-actin Millipore MAB1501R 1:1000, mouse anti-beta-Tubulin Sigma T0198 1:1000, rabbit anti-HA Covance PRB-101P 1:500) and then submitted to detection using a fluorescence coupled antibody (Licor) at a 1:25000 dilution (680 nm rabbit, 800 nm mouse). Membranes were developed using a Odessey (Licor) signal detector. Pictures were then analysed densitometrically using ImageStudioLite 4.0 (Licor).

Analysis of ubiquitylation

For analysis of ubiquitylation, ACTN4 WT or G195D mutant were expressed in 293T cells with HA-tagged ubiquitin, respectively. On the next day, cells were incubated with 10 µM MG132 (Calbiochem) for 1 h before harvest. Cells were washed carefully with PBS. Lysates in 2% SDS buffer containing 150 mM NaCl and 50 mM Tris were boiled for 15 min. Next, cooled lysates were incubated with five times volume of dilution buffer containing 1% NP-40 and Tris. Then, lysates were spun down at 4°C (16000*g*, 20 min). The supernatant was subjected to FLAG-pulldown. The protocol was modified from a previously described version.

For MS analysis of ubiquitylation, lysates were incubated with magnetic µBeads (Miltenyi) and were column purified and subjected to MS/MS analysis as previously described (32). An additional wash with a modified 'ubiquitylation wash buffer' (containing 10 mM Tris–HCl, pH 8.0, 1 M NaCl, 1 mM ethylenediaminetetraacetic acid, 1% NP-40) was introduced after loading the samples. Proteins were reduced, alkylated and digested as described in the co-immunoprecipitation section. The samples were analysed by MS with a 1 h nLC gradient. For analysis of ubiquitylation by immunoblotting, lysates were incubated using anti-FLAG beads and washed with 'ubiquitylation wash buffer' for three times. Then, samples were eluted by boiling in two times Laemmli buffer for 5 min and then analysed using SDS–PAGE and immunoblotting.

Coimmunoprecipitation for MS/MS

For coimmunoprecipitation experiments, two 10 cm dishes of podocytes expressing FLAG-tagged ACTN4 WT and ACTN4 G195D were harvested in one-time modified RIPA buffer containing 1% NP-40 (IgPAL), 150 mM NaCl, 0.25% sodium-deoxycholate and 50 mM Tris. Lysates were cleared using centrifugation (16.000*g*, 20 min at 4°C) and supernatant was incubated with 50 µl of anti-FLAG beads (Miltenyi) for 1 h at 4°C. Subsequently, immunoprecipitated proteins were isolated using magnetic µMACS columns (Miltenyi) as previously described (56). In-column digestion was performed as previously described (32). On the next day, double-layered stage-tip clean up (C18) was performed as described previously (57). Lysates were analysed by MS using a 1 h nLC gradient (see MS analysis). Each experiment was performed in duplicate six times on 3 different days.

Proteomic analysis of WCLs

Primary urinary cells were harvested in PBS and snap-frozen. Pellets were resuspended in cold 8 M Urea, 50 mM ammoniumbicarbonate and one-time protease inhibitor cocktail mix (Roche) and vortexed. Lysates were cleared using centrifugation (16000*g*, 20 min at 4°C). Next, protein lysates were reduced (5 mM dithiothreitol; 45 min), and alkylated (10 mM Iodoacetamide, 45 min in the dark). Then, urea was diluted to 2 M using 50 mM ammoniumbicarbonate and subjected to tryptic digestion. The amount of trypsin was 1:100 wt/wt. Protein amount was measured using a standard bicinchoninic acid assay. Samples were analysed using MS with a 4 h nLC gradient.

nLC and mass spectrometry/mass spectrometry

Peptides (1–5 µg) were separated using a nLC with a 50 cm C18 column (in-house hand-packed, particle size = 1.7 µm) in a column oven (Dr Maisch) as previously described (58). A binary buffer system with buffer A: 0.1% formic acid (FA) and Buffer B 80% Acetonitrile (ACN), 0.1% FA was used. The flow rate was 250 nl/min. The gradient settings were as follows *t* = 0 min; 4% (Buffer B), 05 min, 6%; 125 min, 23%; 132 min, 54%; 138 min, 85%; 143 min, 85% and 145 min 5%. Buffer B was 80% ACN, 0.1% FA

and buffer A was 0.1% FA. The flow rate was constant with 250 nl/min. Peptides were analysed using the quadrupole-orbitrap based QExactive Plus mass spectrometer (Thermo Scientific) (59). The machine was operated in positive ion mode. One survey scan (resolution = 70000, *m*/z 300–1750) was followed by up to 10 MS2 scans (resolution = 17500, *m*/z 200–2000). Dynamic exclusion was enabled (20 s). AGC target was 3e6 for MS1 scans, and 5e5 for MS2 scans.

Bioinformatic analysis

Raw files were searched, quantified and normalized using the MaxQuant version 1.5.0.1 with default settings. The only changed options were: label-free quantification enabled, intensity based absolute quantification (iBAQ) with log fit enabled, match between runs enabled. When ubiquitylation was expected in the sample, the modification K-ε-Gly-Gly on Lysines (ubiquitin remnant) was put as variable modification. The human reference proteome was used as a database. In the human reference proteome (downloaded in June 2014), 5 entries for the gene symbol ACTN4 exist. We found redundancy and unreliable quantification of ACTN4 proteoforms when using the entire database. To make the identification and quantification more stable, the canonical entry (O43707) was chosen, all other, preliminarily annotated proteoforms of the ACTN4 gene were removed from the database. All other proteins were kept in the database. A mutated (G195>D) sequence version of the protein was added to the database to enable identification of the mutated protein sequence. To identify the peptide within the patient sample, a sample of immunopurified ACTN4 G195D was utilized within the library using the match between run option in a 240 min matching window.

MaxQuant output (protein group files, Gly–Gly sites file and modification specific peptides file) were analysed using Perseus 1.5.1.6 or Microsoft Excel. For immunoprecipitation, quantification and stoichiometry statistics were performed as previously described (31,32). Imputation of the missing values was performed when three or more values were present. For analysis of the Gly-Gly sites (ubiquitin remnant), intensities for Gly-Gly sites containing peptides were normalized to the total protein intensity and normalized data were plotted in Microsoft excel. For analysis of the proteomic changes, normalization was performed by subtracting the median from all samples. Then, missing values (when at least three values were present in the data set) were imputed using the normal distribution (downshift 1.8 SD, s0 = 0.3). In all cases, proteins were annotated with GO terms, Pfam (protein families) domains and kyoto encyclopedia of genes and genomes pathways using the Perseus main annotations file (April 2015). Statistical overrepresentation of the respective categories was performed using Fisher's exact test (using a cut-off of $P = 0.05$) and at least three proteins within a category. Cumulative histogram was drawn using GraphPad Prism (v.5). Boxplots have been generated using BoxPlotR (60).

Supplementary Material

Supplementary Material is available at *HMG* online.

Acknowledgements

We thank the patient and her parents for participating in our study, as well as the children and their parents who participated as controls. We thank members of our laboratories for helpful discussion. We thank Stefanie Keller, Ruth Herzog, Astrid Wilbrand-Hennes and Rene Grandjean for excellent technical assistance.

Conflict of Interest statement. None declared.

Funding

This work was supported by Peter Stiftung to S.H., the German Research Foundation DFG to T.B. (SFB829), to B.S. (DFG SCHE 1562/2-1) and M.M.R. (UoC Postdoc grant, Exzellenzinitiative) and intramural grants (Stiftungsgelder, University of Cologne) to B.B.B. and M.M.R.

References

1. Devuyst, O., Knoers, N.V.A.M., Remuzzi, G. and Schaefer, F. and Board of the Working Group for Inherited Kidney Diseases of the European Renal Association and European Dialysis and Transplant Association. (2014) Rare inherited kidney diseases: challenges, opportunities, and perspectives. *Lancet Lond. Engl.*, **383**, 1844–1859.
2. Halbritter, J., Porath, J.D., Diaz, K.A., Braun, D.A., Kohl, S., Chaki, M., Allen, S.J., Soliman, N.A., Hildebrandt, F., Otto, E.A. *et al.* (2013) Identification of 99 novel mutations in a worldwide cohort of 1,056 patients with a nephronophthisis-related ciliopathy. *Hum. Genet.*, **132**, 865–884.
3. Sadowski, C.E., Lovric, S., Ashraf, S., Pabst, W.L., Gee, H.Y., Kohl, S., Engelmann, S., Vega-Warner, V., Fang, H., Halbritter, J. *et al.* (2015) A single-gene cause in 29.5% of cases of steroid-resistant nephrotic syndrome. *J. Am. Soc. Nephrol.*, **26**, 1279–1289.
4. Brown, E.J., Pollak, M.R. and Barua, M. (2014) Genetic testing for nephrotic syndrome and FSGS in the era of next-generation sequencing. *Kidney Int.*, **85**, 1030–1038.
5. Deciphering Developmental Disorders Study. (2015) Large-scale discovery of novel genetic causes of developmental disorders. *Nature*, **519**, 223–228.
6. Francioli, L.C., Polak, P.P., Koren, A., Menelaou, A., Chun, S. and Renkens, I., Genome of the Netherlands Consortium, van Duijn, C.M., Swertz, M., Wijmenga, C. *et al.* (2015) Genome-wide patterns and properties of de novo mutations in humans. *Nat. Genet.*, **47**, 822–826.
7. Gbadegesin, R.A., Winn, M.P. and Smoyer, W.E. (2013) Genetic testing in nephrotic syndrome—challenges and opportunities. *Nat. Rev. Nephrol.*, **9**, 179–184.
8. Kaplan, J.M., Kim, S.H., North, K.N., Rennke, H., Correia, L.A., Tong, H.Q., Mathis, B.J., Rodríguez-Pérez, J.C., Allen, P.G., Beggs, A.H. *et al.* (2000) Mutations in ACTN4, encoding alpha-actinin-4, cause familial focal segmental glomerulosclerosis. *Nat. Genet.*, **24**, 251–256.
9. Pollak, M.R. (2014) Familial FSGS. *Adv. Chronic Kidney Dis.*, **21**, 422–425.
10. Shao, H., Wang, J.H.-C., Pollak, M.R. and Wells, A. (2010) α-Actinin-4 is essential for maintaining the spreading, motility and contractility of fibroblasts. *PLoS One*, **5**, e13921.
11. Tang, V.W. and Brieher, W.M. (2013) FSGS3/CD2AP is a barbed-end capping protein that stabilizes actin and strengthens adherens junctions. *J. Cell Biol.*, **203**, 815–833.
12. Ehrlicher, A.J., Krishnan, R., Guo, M., Bidan, C.M., Weitz, D.A. and Pollak, M.R. (2015) Alpha-actinin binding kinetics modulate cellular dynamics and force generation. *Proc. Natl Acad. Sci. USA*, **112**, 6619–6624.
13. Yao, J., Le, T.C., Kos, C.H., Henderson, J.M., Allen, P.G., Denker, B.M. and Pollak, M.R. (2004) Alpha-actinin-4-mediated FSGS: an inherited kidney disease caused by an aggregated and rapidly degraded cytoskeletal protein. *PLoS Biol.*, **2**, e167.

14. Tang, J., Taylor, D.W. and Taylor, K.A. (2001) The three-dimensional structure of alpha-actinin obtained by cryoelectron microscopy suggests a model for Ca(2+)-dependent actin binding. *J. Mol. Biol.*, **310**, 845–858.
15. Djinović-Carugo, K., Young, P., Gautel, M. and Saraste, M. (1999) Structure of the alpha-actinin rod: molecular basis for cross-linking of actin filaments. *Cell*, **98**, 537–546.
16. Dandapani, S.V., Sugimoto, H., Matthews, B.D., Kolb, R.J., Sinha, S., Gerszten, R.E., Zhou, J., Ingber, D.E., Kalluri, R. and Pollak, M.R. (2007) Alpha-actinin-4 is required for normal podocyte adhesion. *J. Biol. Chem.*, **282**, 467–477.
17. Zhao, X., Hsu, K.-S., Lim, J.H., Bruggeman, L.A. and Kao, H.-Y. (2015) α-Actinin 4 potentiates nuclear factor κ-light-chain-enhancer of activated B-cell (NF-κB) activity in podocytes independent of its cytoplasmic actin binding function. *J. Biol. Chem.*, **290**, 338–349.
18. Nakatsuji, H., Nishimura, N., Yamamura, R., Kanayama, H.-O. and Sasaki, T. (2008) Involvement of actinin-4 in the recruitment of JRAB/MICAL-L2 to cell-cell junctions and the formation of functional tight junctions. *Mol. Cell. Biol.*, **28**, 3324–3335.
19. Lehtonen, S., Ryan, J.J., Kudlicka, K., Iino, N., Zhou, H. and Farquhar, M.G. (2005) Cell junction-associated proteins IQGAP1, MAGI-2, CASK, spectrins, and alpha-actinin are components of the nephrin multiprotein complex. *Proc. Natl Acad. Sci. USA*, **102**, 9814–9819.
20. Weins, A., Kenlan, P., Herbert, S., Le, T.C., Villegas, I., Kaplan, B.S., Appel, G.B. and Pollak, M.R. (2005) Mutational and biological analysis of alpha-actinin-4 in focal segmental glomerulosclerosis. *J. Am. Soc. Nephrol.*, **16**, 3694–3701.
21. Michaud, J.-L.R., Chaisson, K.M., Parks, R.J. and Kennedy, C.R.J. (2006) FSGS-associated alpha-actinin-4 (K256E) impairs cytoskeletal dynamics in podocytes. *Kidney Int.*, **70**, 1054–1061.
22. Weins, A., Schlondorff, J.S., Nakamura, F., Denker, B.M., Hartwig, J.H., Stossel, T.P. and Pollak, M.R. (2007) Disease-associated mutant alpha-actinin-4 reveals a mechanism for regulating its F-actin-binding affinity. *Proc. Natl Acad. Sci. USA*, **104**, 16080–16085.
23. Feng, D., DuMontier, C. and Pollak, M.R. (2015) The role of alpha-actinin-4 in human kidney disease. *Cell Biosci.*, **5**, 44.
24. McDaniell, R., Warthen, D.M., Sanchez-Lara, P.A., Pai, A., Krantz, I.D., Piccoli, D.A. and Spinner, N.B. (2006) NOTCH2 mutations cause Alagille syndrome, a heterogeneous disorder of the notch signaling pathway. *Am. J. Hum. Genet.*, **79**, 169–173.
25. Zhou, T., Benda, C., Dunzinger, S., Huang, Y., Ho, J.C., Yang, J., Wang, Y., Zhang, Y., Zhuang, Q., Li, Y. *et al.* (2012) Generation of human induced pluripotent stem cells from urine samples. *Nat. Protoc.*, **7**, 2080–2089.
26. Henderson, J.M., Alexander, M.P. and Pollak, M.R. (2009) Patients with ACTN4 mutations demonstrate distinctive features of glomerular injury. *J. Am. Soc. Nephrol.*, **20**, 961–968.
27. Lee, S.H., Weins, A., Hayes, D.B., Pollak, M.R. and Dominguez, R. (2008) Crystal structure of the actin-binding domain of alpha-actinin-4 Lys255Glu mutant implicated in focal segmental glomerulosclerosis. *J. Mol. Biol.*, **376**, 317–324.
28. Franzot, G., Sjöblom, B., Gautel, M. and Djinović Carugo, K. (2005) The crystal structure of the actin binding domain from alpha-actinin in its closed conformation: structural insight into phospholipid regulation of alpha-actinin. *J. Mol. Biol.*, **348**, 151–165.
29. Borrego-Diaz, E., Kerff, F., Lee, S.H., Ferron, F., Li, Y. and Dominguez, R. (2006) Crystal structure of the actin-binding domain of alpha-actinin 1: evaluating two competing actin-binding models. *J. Struct. Biol.*, **155**, 230–238.
30. Udeshi, N.D., Mertins, P., Svinkina, T. and Carr, S.A. (2013) Large-scale identification of ubiquitination sites by mass spectrometry. *Nat. Protoc.*, **8**, 1950–1960.
31. Smits, A.H., Jansen, P.W.T.C., Poser, I., Hyman, A.A. and Vermeulen, M. (2013) Stoichiometry of chromatin-associated protein complexes revealed by label-free quantitative mass spectrometry-based proteomics. *Nucleic Acids Res.*, **41**, e28.
32. Kohli, P., Bartram, M.P., Habbig, S., Pahmeyer, C., Lamkemeyer, T., Benzing, T., Schermer, B. and Rinschen, M.M. (2014) Label-free quantitative proteomic analysis of the YAP and TAZ interactome. *Am. J. Physiol. Cell Physiol.*, doi:10.1152/ajpcell.00339.2013.
33. Schwanhäusser, B., Busse, D., Li, N., Dittmar, G., Schuchhardt, J., Wolf, J., Chen, W. and Selbach, M. (2011) Global quantification of mammalian gene expression control. *Nature*, **473**, 337–342.
34. Vissers, L.E.L.M., de Ligt, J., Gilissen, C., Janssen, I., Steehouwer, M., de Vries, P., van Lier, B., Arts, P., Wieskamp, N., del Rosario, M. *et al.* (2010) A de novo paradigm for mental retardation. *Nat. Genet.*, **42**, 1109–1112.
35. Ng, S.B., Buckingham, K.J., Lee, C., Bigham, A.W., Tabor, H.K., Dent, K.M., Huff, C.D., Shannon, P.T., Jabs, E.W., Nickerson, D.A. *et al.* (2010) Exome sequencing identifies the cause of a Mendelian disorder. *Nat. Genet.*, **42**, 30–35.
36. Cassa, C.A., Tong, M.Y. and Jordan, D.M. (2013) Large numbers of genetic variants considered to be pathogenic are common in asymptomatic individuals. *Hum. Mutat.*, **34**, 1216–1220.
37. Heller, R. and Bolz, H.J. (2015) The challenge of defining pathogenicity: the example of AHI1. *Genet. Med.*, **17**, 508.
38. Elsayed, S.M., Phillips, J.B., Heller, R., Thoenes, M., Elsobky, E., Nürnberg, G., Nürnberg, P., Seland, S., Ebermann, I., Altmüller, J. *et al.* (2015) Non-manifesting AHI1 truncations indicate localized loss-of-function tolerance in a severe Mendelian disease gene. *Hum. Mol. Genet.*, **24**, 2594–2603.
39. 1000 Genomes Project ConsortiumAbecasis, G.R., Auton, A., Brooks, L.D., DePristo, M.A., Durbin, R.M., Handsaker, R.E., Kang, H.M., Marth, G.T. and McVean, G.A. (2012) An integrated map of genetic variation from 1,092 human genomes. *Nature*, **491**, 56–65.
40. Ajzenberg, H., Slaats, G.G., Stokman, M.F., Arts, H.H., Logister, I., Kroes, H.Y., Renkema, K.Y., van Haelst, M.M., Terhal, P.A., van Rooij, I.A. *et al.* (2015) Non-invasive sources of cells with primary cilia from pediatric and adult patients. *Cilia*, **4**, 8.
41. Hall, A. (1998) Rho GTPases and the actin cytoskeleton. *Science*, **279**, 509–514.
42. Maul, R.S., Song, Y., Amann, K.J., Gerbin, S.C., Pollard, T.D. and Chang, D.D. (2003) EPLIN regulates actin dynamics by cross-linking and stabilizing filaments. *J. Cell Biol.*, **160**, 399–407.
43. Vallenius, T., Luukko, K. and Mäkelä, T.P. (2000) CLP-36 PDZ-LIM protein associates with nonmuscle alpha-actinin-1 and alpha-actinin-4. *J. Biol. Chem.*, **275**, 11100–11105.
44. Schmeichel, K.L. and Beckerle, M.C. (1994) The LIM domain is a modular protein-binding interface. *Cell*, **79**, 211–219.
45. Bijian, K., Takano, T., Papillon, J., Le Berre, L., Michaud, J.-L., Kennedy, C.R.J. and Cybulsky, A.V. (2005) Actin cytoskeleton regulates extracellular matrix-dependent survival signals in glomerular epithelial cells. *Am. J. Physiol. Renal Physiol.*, **289**, F1313–F1323.
46. Kadrmas, J.L. and Beckerle, M.C. (2004) The LIM domain: from the cytoskeleton to the nucleus. *Nat. Rev. Mol. Cell Biol.*, **5**, 920–931.

47. Alfaro, J.A., Sinha, A., Kislinger, T. and Boutros, P.C. (2014) Onco-proteogenomics: cancer proteomics joins forces with genomics. *Nat. Methods*, **11**, 1107–1113.
48. Zhang, B., Wang, J., Wang, X., Zhu, J., Liu, Q., Shi, Z., Chambers, M.C., Zimmerman, L.J., Shaddox, K.F., Kim, S. *et al.* (2014) Proteogenomic characterization of human colon and rectal cancer. *Nature*, **513**, 382–387.
49. Budde, B.S., Mizumoto, S., Kogawa, R., Becker, C., Altmüller, J., Thiele, H., Rüschendorf, F., Toliat, M.R., Kaleschke, G., Hämmerle, J.M. *et al.* (2015) Skeletal dysplasia in a consanguineous clan from the island of Nias/Indonesia is caused by a novel mutation in B3GAT3. *Hum. Genet.*, **134**, 691–704.
50. Kent, W.J., Sugnet, C.W., Furey, T.S., Roskin, K.M., Pringle, T.H., Zahler, A.M. and Haussler, D. (2002) The human genome browser at UCSC. *Genome Res.*, **12**, 996–1006.
51. Rosenbloom, K.R., Armstrong, J., Barber, G.P., Casper, J., Clawson, H., Diekhans, M., Dreszer, T.R., Fujita, P.A., Guruvadoo, L., Haeussler, M. *et al.* (2015) The UCSC Genome Browser database: 2015 update. *Nucleic Acids Res.*, **43**, D670–D681.
52. Schwarz, J.M., Rödelsperger, C., Schuelke, M. and Seelow, D. (2010) MutationTaster evaluates disease-causing potential of sequence alterations. *Nat. Methods*, **7**, 575–576.
53. Adzhubei, I.A., Schmidt, S., Peshkin, L., Ramensky, V.E., Gerasimova, A., Bork, P., Kondrashov, A.S. and Sunyaev, S.R. (2010) A method and server for predicting damaging missense mutations. *Nat. Methods*, **7**, 248–249.
54. Saleem, M.A., O'Hare, M.J., Reiser, J., Coward, R.J., Inward, C.D., Farren, T., Xing, C.Y., Ni, L., Mathieson, P.W. and Mundel, P. (2002) A conditionally immortalized human podocyte cell line demonstrating nephrin and podocin expression. *J. Am. Soc. Nephrol.*, **13**, 630–638.
55. Michaud, J.-L.R., Hosseini-Abardeh, M., Farah, K. and Kennedy, C.R.J. (2009) Modulating alpha-actinin-4 dynamics in podocytes. *Cell Motil. Cytoskeleton*, **66**, 166–178.
56. Hubner, N.C. and Mann, M. (2011) Extracting gene function from protein-protein interactions using Quantitative BAC InteraCtomics (QUBIC). *Methods San Diego Calif*, **53**, 453–459.
57. Rappsilber, J., Ishihama, Y. and Mann, M. (2003) Stop and go extraction tips for matrix-assisted laser desorption/ionization, nanoelectrospray, and LC/MS sample pretreatment in proteomics. *Anal. Chem.*, **75**, 663–670.
58. Rinschen, M.M., Wu, X., König, T., Pisitkun, T., Hagmann, H., Pahmeyer, C., Lamkemeyer, T., Kohli, P., Schnell, N., Schermer, B. *et al.* (2014) Phosphoproteomic analysis reveals regulatory mechanisms at the kidney filtration barrier. *J. Am. Soc. Nephrol.*, doi: 10.1681/ASN.2013070760.
59. Michalski, A., Damoc, E., Hauschild, J.-P., Lange, O., Wieghaus, A., Makarov, A., Nagaraj, N., Cox, J., Mann, M. and Horning, S. (2011) Mass spectrometry-based proteomics using Q Exactive, a high-performance benchtop quadrupole Orbitrap mass spectrometer. *Mol. Cell. Proteomics*, **10**, M111.011015.
60. Spitzer, M., Wildenhain, J., Rappsilber, J. and Tyers, M. (2014) BoxPlotR: a web tool for generation of box plots. *Nat. Methods*, **11**, 121–122.
61. Parthiban, V., Gromiha, M.M. and Schomburg, D. (2006) CUPSAT: prediction of protein stability upon point mutations. *Nucleic Acids Res.*, **34**, W239–W242.
62. Yin, S., Ding, F. and Dokholyan, N.V. (2007) Eris: an automated estimator of protein stability. *Nat. Methods*, **4**, 466–467.
63. Capriotti, E., Fariselli, P. and Casadio, R. (2005) I-Mutant2.0: predicting stability changes upon mutation from the protein sequence or structure. *Nucleic Acids Res.*, **33**, W306–W310.
64. Dehouck, Y., Grosfils, A., Folch, B., Gilis, D., Bogaerts, P. and Rooman, M. (2009) Fast and accurate predictions of protein stability changes upon mutations using statistical potentials and neural networks: PoPMuSiC-2.0. *Bioinforma. Oxf. Engl.*, **25**, 2537–2543.
65. Dehouck, Y., Kwasigroch, J.M., Gilis, D. and Rooman, M. (2011) PoPMuSiC 2.1: a web server for the estimation of protein stability changes upon mutation and sequence optimality. *BMC Bioinformatics*, **12**, 151.
66. Pires, D.E.V., Ascher, D.B. and Blundell, T.L. (2014) DUET: a server for predicting effects of mutations on protein stability using an integrated computational approach. *Nucleic Acids Res.*, **42**, W314–W319.